

OMAE2022-79413

ON SOME NONLINEAR WAVE DIFFRACTION AND REFRACTION
SOLUTIONS IN SHALLOW WATERS

Masoud Hayatdavoodi

Civil Engineering Department

University of Dundee

Dundee, DD1 4HN, UK

& College of Shipbuilding Engineering

Harbin Engineering University

Harbin, China

Email: mhayatdavoodi@dundee.ac.uk

R. Cengiz Ertekin

Ocean and Resources Engineering Department

University of Hawaii at Manoa

Honolulu, HI 96822, USA

& College of Shipbuilding Engineering

Harbin Engineering University

Harbin, China

Email: ertekin@hawaii.edu

1 **ABSTRACT**

2 *Diffraction and refraction of nonlinear shallow water*
3 *waves due to uneven bathymetry is studied numerically in*
4 *two and three dimensions. The numerical tank consists of*
5 *a wavemaker at the upwave side of the domain, the sub-*
6 *merged obstacles in the middle of the domain, and a nu-*
7 *merical wave absorber on the downwave of the domain.*
8 *The numerical wavemaker is capable of generating solitary*
9 *and cnoidal waves as solutions of the Green-Naghdi (GN)*
10 *equations. The nonlinear wave refraction and diffraction*
11 *is studied by use of the Level I GN equations. The sys-*
12 *tem of equations are solved numerically in time domain by*
13 *use of a second-order finite difference approach, and in a*
14 *boundary-fitted coordinate system. Various forms of three-*
15 *dimensional bathymetry with large slopes, including flat*
16 *and curved ramps from deep to shallow regions are con-*
17 *sidered. Results include solitary and cnoidal wave surface*
18 *elevation and particle velocities and are compared with the*
19 *existing solutions where possible. Overall very good agree-*
20 *ment is observed. Discussion is provided on the nonlinear-*
21 *ity and dispersion effects on the wave diffraction and re-*
22 *fraction, as well as on the performance of the GN equations*
23 *in solving these problems.*

24 **Keywords:** Nonlinear waves, wave refraction and
25 diffraction, Green-Naghdi equations, soliton fission

26 **Introduction**

27 Wave diffraction and refraction are subjects of great in-
28 terest to ocean engineers. The linear wave theory, based on
29 the assumption of small amplitude waves, provides solu-
30 tions to wave diffraction and refraction in the presence of
31 simplified bathymetry and geometries. In shallow waters,
32 however, the water depth is much less than the wavelength,
33 and the wave amplitude is not necessarily small when com-
34 pared to the water depth, and hence the assumption of a
35 linear free-surface boundary condition is no longer appli-
36 cable. Due to the change in water depth, the long waves
37 undergo significant transformation. The original, nearly si-
38 nusoidal, wave profile transforms into waves of long and
39 flat troughs and isolated and rather sharp crests as they en-
40 ter shallow waters. The wave height, speed and direction
41 of propagation would also change significantly, and these
42 vary with the spatial form of the bathymetry. Such defor-
43 mations continue as the water depth decreases, to the limit
44 that the wave becomes asymmetric about its crest and even-
45 tually leads to instabilities resulting in energy attenuation,
46 formation of higher harmonics, and possibly wave break-
47 ing. The nonlinear effects resulting in such wave transfor-
48 mations cannot be captured by the simplified linear free-
49 surface boundary conditions. Climate change and its im-
50 pact on frequency and intensity of extreme events, and the

51 sea-level rise, add to the importance of development of ap- 100
52 proaches that can realistically and efficiently analyse the 101
53 wave transformation in coastal areas. 102

54 A common approach to model the nonlinear free- 103
55 surface boundary condition is to assume that certain im- 104
56 portant features of the fluid domain remain unchanged dur- 105
57 ing the wave transformation, and obtain an approximate so- 106
58 lution for the nonlinear boundary conditions. In shallow 107
59 waters, this is achieved by introducing two major scales, 108
60 namely nonlinearity (the ratio of wave height to water 109
61 depth, $\sigma = H/h$) and dispersion (the ratio of water depth 110
62 to wavelength, $\varepsilon = h/\lambda$). The unknowns (typically the ve- 111
63 locity potential and the free surface) are expanded into a 112
64 perturbation series ordered in terms of σ and ε , the scales 113
65 or perturbation parameters, typically assumed small from 114
66 the outset. It is then possible for one to decide whether 115
67 σ or ε is more critical, and which terms in the expansion 116
68 are to be retained and which terms can be discarded, deter- 117
69 mined based on the physical problem, and hence obtain 118
70 an approximate solution to the exact problem. This is the 119
71 “classical perturbation method” in water wave mechanics, 120
72 and is followed by [1–8] and several others afterwards to 121
73 obtain various form of theories for nonlinear wave propaga- 122
74 tion in shallow waters. All methods, following the pertur- 123
75 bation approach, arrive at similar, but not identical, equa- 124
76 tions for propagation of long waves. Models developed for 125
77 wave diffraction and refraction in shallow water based on 126
78 these approaches are discussed in [9–13], among others. 127

79 Green and Naghdi [14] proposed yet another funda- 128
80 mentally different approach in studying nonlinear wave 129
81 transformation in shallow waters based on a *continuum* 130
82 *model* typically applied to the theory of plates and shells in 131
83 structural mechanics. The theory is developed based on the 132
84 directed or Cosserat surface, a deformable surface embed- 133
85 ded in a Euclidean three-dimensional space to every point 134
86 of which a deformable vector, called a director, is assigned. 135
87 The Cosserat surface is three-dimensional in character, but 136
88 only depends on two spatial dimensions and time. The di- 137
89 rectors of the Cosserat surface specify how certain proper- 138
90 ties are distributed in the third dimension of the *continuum*
91 *model*. In this theory, the number of the directors defines 139
92 the *Level* of the theory. 140

93 In the Level I theory, used in this study, the deformable 141
94 medium is a body of sheet-like fluid consisting of a de- 142
95 formable top (free) surface and a single director attached 143
96 to each point of the surface. This assumption, which is 144
97 the only assumption made about the kinematics of the fluid 145
98 sheet, is equivalent to the linear distribution of the vertical 146
99 velocity along the water column, and hence (due to the con- 147

tinuity equation) the horizontal velocity becomes invariant 100
over the water depth. This makes the Level I theory mostly 101
applicable to propagation of long waves. 102

Given that no perturbation is used in the derivation of 103
the Green-Naghdi (GN hereafter) equations, there is no re- 104
striction on any scaling ratio, e.g., wave amplitude over the 105
wave length, or alike in this approach, unlike the classical 106
approximations. The only restriction on the thickness of the 107
fluid sheet is that it is finite, and nonzero (zero water depth 108
leads to a singularity in the equations). There is no need 109
to define velocity potential and hence irrotationality of the 110
flow is not necessary either. The GN equations are transla- 111
tionally (Galilean) invariant (unlike the equations presented 112
by [3], among others), satisfy the nonlinear boundary con- 113
ditions and the conservation of mass exactly, and postulate 114
the integrated momentum equation. 115

Further flexibility can be given to the directors when 116
deriving the GN equations. This can be achieved by as- 117
suming higher order functions (polynomial or exponential) 118
for the distribution of the vertical velocity along the water 119
column. High-level GN equations are applicable to wave 120
propagation in any water depth, see e.g. [15–18]. We note 121
that the boundary conditions are satisfied exactly by the GN 122
equations of any level. That is, the only difference between 123
the GN equations of different levels is on the velocity field. 124

In this paper, we investigate the effects of spatial 125
changes of the bathymetry on the propagation of nonlin- 126
ear waves in shallow water by use of the Level I GN equa- 127
tions. The model will allow studying the wave transforma- 128
tion while preserving the effect of nonlinearity, dispersion 129
and wave reflection (i.e. no need to restrict the wave motion 130
to one direction only). Various forms of bottom bathymetry 131
with three dimensional (3D) effects on the wave field are 132
considered and discussion is provided on the wave trans- 133
formation. The theory and the solution are discussed first, 134
followed by an introduction to the physical problems under 135
consideration. Results of solitary and cnoidal wave diffrac- 136
tion and refraction are presented and discussed next and the 137
paper is closed by concluding remarks. 138

139 The Green-Naghdi Equations

140 For an incompressible and inviscid fluid, Green and 141
Naghdi [19] showed that it is possible to derive the gov- 142
erning equations in a systematic way from the exact three- 143
dimensional equations of an incompressible, inviscid fluid 144
(Euler’s equations) by use of a single approximation for 145
the (three-dimensional) velocity field. The assumption is 146
equivalent to the Level I assumption in the direct approach, 147
that is the vertical component of the velocity field is a lin-

ear function of the vertical coordinate (in a Eulerian system) and that the horizontal components are invariable in the vertical direction. Such a velocity field allows for rotational flow on the horizontal surface, and the vorticity component on the horizontal plane does not need to be zero even though the shear flow on the vertical surfaces are ignored.

We use a Cartesian coordinate system (x_1, x_2, x_3) , with the associated orthonormal base vectors e_i , such that the $x_1 - x_3$ plane is the still-water level (SWL) and e_2 is vertically upward. The mass density ρ of the fluid and the gravitational acceleration g , in the $-e_2$ direction, are constant. Subscripts after comma designate partial differentiation with respect to time or the corresponding spatial direction. Ertekin [20] provided a familiar form of the equations given by the mass and momentum conservation as

$$\eta_{,t} + \{(h + \eta - \alpha)u_j\}_{,j} = \alpha_{,t}, \quad j = 1, 3, \quad (1)$$

$$\begin{aligned} \dot{u}_i + g\eta_{,i} + \frac{\hat{p}_{,i}}{\rho} = & -\frac{1}{6}\{[2\eta + \alpha]_{,i}\ddot{\alpha} + [4\eta - \alpha]_{,i}\ddot{\eta} \\ & + (h + \eta - \alpha)[\ddot{\alpha} + 2\ddot{\eta}]_{,i}\}, \quad j = 1, 3, \quad (2) \end{aligned}$$

where $V = u_1e_1 + u_2e_2 + u_3e_3$ is the velocity vector, $\eta(x_1, x_3, t)$ is the free surface elevation measured from the SWL, $\alpha(x_1, x_3, t)$ describes the seafloor surface, and t is the time variable. The scalar function $\hat{p}(x_1, x_3, t)$ is the fluid pressure on the top surface, and $h(x_1, x_3)$ is the water depth (measured from the SWL to the stationary seafloor). The superposed dot denotes the material derivative, and a double superposed dot is defined as the second material time derivative. With no loss in generality, in this study we confine our attention to cases where (i) the seafloor is stationary, i.e. $\alpha(x_1, x_3, t) = \alpha(x_1, x_3)$, and (ii) $\hat{p}(x_1, x_3, t) = 0$, i.e. pressure is atmospheric on the top surface. Breaking waves are excluded from this study.

Numerical Solution and Setup

A 3D numerical wave channel is created, where a wavemaker is placed on one end and a wave absorber is located at the opposite end. The numerical wavemaker generates solitary and cnoidal waves of the GN equations, see [20] and [21]. The open-boundary uses Orlandi's condition applied to both surface elevation and horizontal velocity to reduce reflections back into the wave tank.

The exact nonlinear free surface (kinematic and dynamic) and the seafloor boundary conditions are embedded within the GN equations (1) to (2). On the lateral sides of the wave tank, the channel walls, two types of boundary conditions are enforced, namely the wall condition for no

flux normal to the walls, and the radiation condition based on the assumption that the velocity and surface elevation vary smoothly near the lateral boundary to minimize the effect of the lateral walls on the flow field (when the wave refraction and flow in the x_3 direction are remarkable near the wall), see [22] for more details.

The system of equations are solved by use of a central difference method, second order in space, see [20] for more details. A numerical grid generation is applied to facilitate the use of finite-difference method to solve the equations in the presence of irregular boundaries. This allows the inclusion of irregular boundaries conveniently by mapping the physical domain into a rectangular computational domain. An elliptical mesh generation technique is used, in which a one-to-one mapping is developed between the physical and the computational planes by use of the Laplace equation. A uniform computational grid system with unit interval spacings is used in the solution of all the governing equations, which significantly simplifies the use of finite-difference method, see [23] for more details.

All problems considered here are symmetric with respect to the $x_1 - x_2$ plane passing through the center line of the domain, and hence only one half of the domain is analyzed by use of the symmetry condition. To avoid numerical instabilities, the bathymetry of the cases considered here are slightly smoothed by taking a weighted average of the depth values of the neighboring points.

Time marching of the solution is achieved iteratively by use of the successive over-relaxation method, see [24] for more details. Hereafter, all variables are given in dimensionless form by use of ρ , g and h (water depth upwave of the ramp) as a dimensionally independent set. A spatial grid with $\Delta x_1 = \Delta x_3 = 0.4$ is used for domain discretization. A time step of $\Delta t = 0.4$ is used for all calculations, see [22] and [25] for discussion on the grid convergence.

The GN model, discussed in this study, has been verified and validated previously for wave propagation over various forms of uneven bathymetry in two dimensions by [21, 26, 27] for solitary and cnoidal waves propagation over submerged ramps, bumps and mounts. Results of the equations have also been extensively compared with laboratory experiments for wave deformation due fixed or floating bodies, see e.g. [23, 24, 28–30]. In this paper, we will build upon the previous investigations of [22], and confine our attention to the results of the GN model for nonlinear wave diffraction and refraction.

227 **Results and Discussion**

228 We consider propagation of nonlinear waves of solitary
 229 and cnoidal types over a bottom shelf. The shelf consists
 230 of a 1:20 flat, linear ramp (FLR hereafter), gradually
 231 connecting the constant water depth to shallow region, whose
 232 dimensions are shown in Fig. 1. To better investigate
 233 the 3D effects and wave refraction, we extend the FLR by
 234 adding an additional component across the shelf and con-
 235 sider another four curved-bottom ramps, namely (i) narrow
 236 concave ramp (NCR), (ii) wide concave ramp (WCR), (iii)
 237 narrow convex ramp (NXR), and (iv) wide convex ramp
 238 (WXR), whose dimensions are shown in Fig. 1. The 3D
 239 ramp profile, varying both in x_1 and x_3 directions, is given
 240 by $f(x_3) = A_R \cos^2(2\pi x_3/B_R)$ for $x_3 \leq B_R$, where A_R and
 241 B_R are the curve amplitude and width of the 3D curves of
 242 the ramp, respectively, whose values are given in Table 1
 243 (also shown in Fig. 1). These are similar to those consid-
 244 ered by [25], who used Boussinesq-class equations to study
 245 the wave refraction and diffraction.

TABLE 1. Amplitude and width of the ramp curves

Case	FLR	NCR	WCR	NXR	WXR
A_R	0	10	10	-10	-10
B_R	0	12	24	12	24

246 In all cases, the domain length is 120, extended from
 247 $x_1 = -30$ to $x_1 = 90$, and its width is 32, from $x_3 = 16$ to
 248 $x_3 = -16$. $x_3 = 0$, the center line of the bathymetry, is the
 249 line of symmetry in all cases. The ramp starts from $x_1 = 6$,
 250 and the water depth on the shelf (downwave of the ramp) is
 251 always $h_1 = 0.5$.

252 **Solitary Waves**

253 The solitary wave amplitude is kept constant in all
 254 cases considered in this study at $A = 0.12$. The 3D sur-
 255 face elevation of the waves propagating over the five ramps
 256 are shown in Fig. 2. The color bar remains unchanged in all
 257 cases for better comparisons. The wave profile undergoes
 258 significant deformation as it propagates over the shelves.

259 The nonlinearity parameter, σ , is physically mani-
 260 fested as the tendency of the wave front to steepen during
 261 the propagation, while the dispersion parameter, ε , gauges
 262 the tendency of a single wave to disperse into a train of
 263 oscillatory waves. The relative magnitude of these two pa-
 264 rameters, the Ursell number $Ur = \sigma/\varepsilon^2$, is often used to
 265 determine which phenomenon (nonlinearity or dispersion)
 266 dominates during the wave transformation, see [31]. The
 267 wave is stable when the two parameters are in balance, i.e.
 268 $Ur = \mathcal{O}(1)$. The change in the bathymetry breaks this bal-

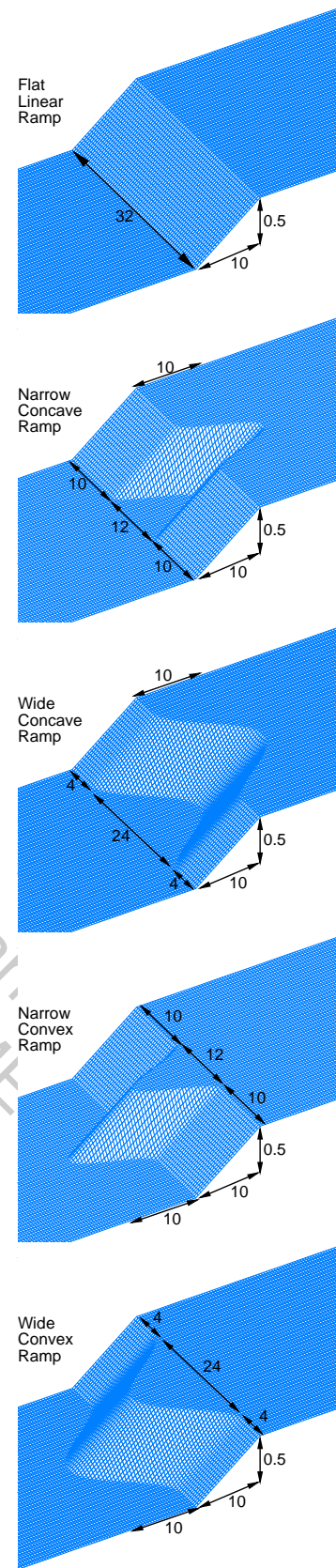


FIGURE 1. Schematic of the five deep-to-shallow ramps considered in this study, and their dimensions. Not to scale.

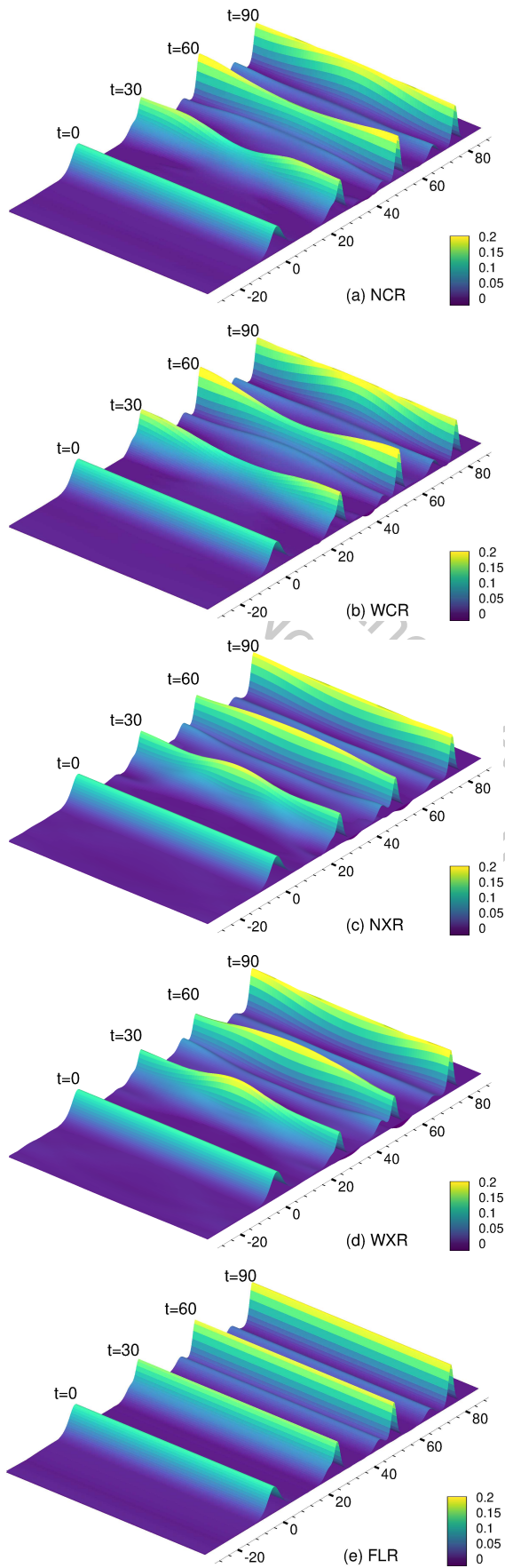


FIGURE 2. Snapshots of the surface elevation of a solitary wave propagating over (a) NCR, (b) WCR, (c) NXR, (d) WXR, and (e) FLR. The ramp starts from $x_1 = 6$. The snapshots are taken at four different times, but plotted on the same figure.

269 ance locally, and hence the wave undergoes deformation to
270 achieve a new stable form.

271 As the wave approaches the ramp, part of the mass
272 and energy is reflected back, and the wave deformation be-
273 gins. Water depth reduces as the wave propagates over the
274 ramp and onto the shelf, resulting in increasing nonlinear-
275 ity. Hence, in all cases, the amplitude of the main soliton
276 is larger immediately downwave of the shelf. As the wave
277 propagates away from the shelf, dispersion comes to play
278 and results in formation of second and third solitons, which
279 separate from the main wave as it propagates over the con-
280 stant water depth above the shelf. The form of the 3D shelf,
281 of course, plays an important role on the exact form and
282 amplitude of the solitons.

283 Comparing results of the FLR case to the other four
284 clearly shows the 3D effects, causing asymmetry of the
285 wave profile from the center line ($x_3 = 0$) and the wall of
286 the domain ($x_3 = 16$), best seen in snapshots taken at times
287 $t = 30$ and 60 in Fig. 2 (a) - (d). In the concave ramp cases,
288 NCR and WCR, the amplitude of the main soliton becomes
289 larger along the wall, while for the convex cases, NXR and
290 WXR, the main soliton's peak is amplified along the center-
291 line of the domain. This is in line with the classic wave
292 refraction theories (see e.g. [32]), where the lines parallel
293 to the wave crest, obliquely approaching a ramp, turn di-
294 rection such that the angle between the crest line and the
295 depth contours become smaller, i.e. Snell's law. Similarly,
296 in the 3D ramps, the ray lines (lines perpendicular to the
297 3D wave crest pointing to the wave propagation direction)
298 turn towards shallower water as the wave passes over the
299 curved ramp.

300 The cases with wider curved ramps, WCR and WXR,
301 cause larger differences of the wave amplitude across the
302 channels when compared to the cases with narrower ramps,
303 NCR and NXR. Downwave from the shelf and over the
304 constant water depth, the balance between nonlinearity and
305 dispersion is achieved once again and the wave profile be-
306 comes nearly identical across the channel, best seen in
307 snapshots taken at time $t = 60$ in Fig. 2 (a)-(d).

308 To better assess the effect of the uneven seafloor on the
309 wave field, in Fig. 3, we look at the snapshots of the verti-
310 cal velocity at the free surface taken at four different times.
311 When compared to the flat linear ramp (FLR), the distribu-
312 tion of the vertical velocity is asymmetric from the center
313 line of the channel to the channel walls. As the wave de-
314 forms, in the concave cases, NCR and WCR, areas of nega-
315 tive vertical velocity is observed at the back of the wave
316 (best seen at time $t = 60$ in Fig. 3 (a) and (b)), which have
317 larger magnitudes in the wider ramp case, WCR. The op-

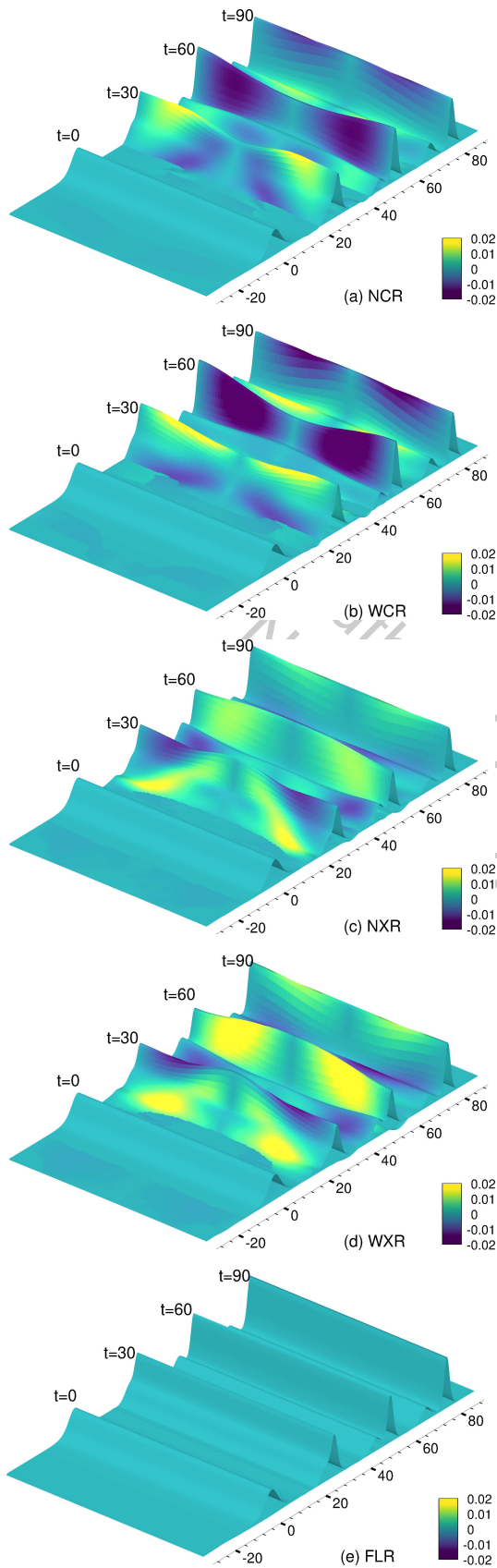


FIGURE 3. Snapshots of the vertical velocity of a solitary wave propagating over (a) NCR, (b) WCR, (c) NXR, (d) WXR, and (e) FLR. The snapshots are taken at four different times, but plotted on the same figure. The color bars are kept the same in all figures to allow for better comparisons between cases.

318 positive is observed in these regions for the convex cases, i.e.
 319 larger positive vertical velocities, which are more remark-
 320 able in the wider ramp case, WXR. The horizontal velocity
 321 (not shown here due to page limits) is always larger at areas
 322 with larger surface elevation.

323 To better investigate the change in the wave profile
 324 across the width of the channels (due to the curved ramps),
 325 in Figs. 4 to 8, we look at snapshots of surface elevation
 326 across the center line and the wall of the channel. We keep
 327 the height of the vertical axis the same in all these figures
 328 for better comparisons. In all cases, as mentioned earlier,
 329 the front side of the wave steepens and the wave amplitude
 330 grows as the wave approaches the ramp. Downwave over
 331 the shelf, soliton fission is observed, where two or three
 332 solitons are formed and as the wave propagates, separate
 333 from the leading soliton due to differences in their propa-
 334 gation velocity (note that the soliton speed is $U = \sqrt{1+A}$,
 335 always critical or supercritical).

336 When compared to the FLR case, in all curved cases,
 337 there is a remarkable difference between the wave profile at
 338 the center of the domain versus that at the channel wall, best
 339 seen at times $t = 40$ and 60 in Figs. 4 to 7, which, is due
 340 to the wave refraction by the different curved bathymetry.
 341 In the concave cases, NCR and WCR, the wave amplitude
 342 is larger near the wall, and the opposite is observed for the
 343 convex cases, NXR and WXR. At the later stages of soliton
 344 propagation over the shelf, $t = 80$ in Figs. 4 to 7, the ampli-
 345 tude of the main solitons are nearly identical at the center
 346 and wall cut of the channel. The amplitude of the second
 347 and third solitons, however, are different at the center and
 348 wall cut of the channel even at $t = 80$; in the concave cases,
 349 the amplitude of the second soliton is larger at the center
 350 line, while the opposite is observed in the convex cases.
 351 Similarly, in the concave cases, at time $t = 80$, the second
 352 soliton is separated from the main soliton at the center line
 353 of the domain while it is still part of the main soliton at the
 354 channel wall. In the convex cases, the opposite is observed,
 355 i.e. the second soliton at the wall is separated, but not at the
 356 center line.

357 Shown in Figs. 4 to 8, results of the GN equations
 358 are in very good agreement with those obtained by [25]
 359 by use of the Boussinesq equations. Results of the solitary
 360 wave propagating over FLR, shown in Fig. 8, are
 361 also in good agreement with the laboratory measurements
 362 of Madsen and Mei [5] (who report 1.66 and 0.75 for the
 363 amplitude of the first and second solitons, respectively)
 364 and calculations of Johnson [33] (who reports 1.71 and
 365 0.66 for the amplitudes of the first and second solitons, re-
 366 spectively), although the peak of the soliton calculated by

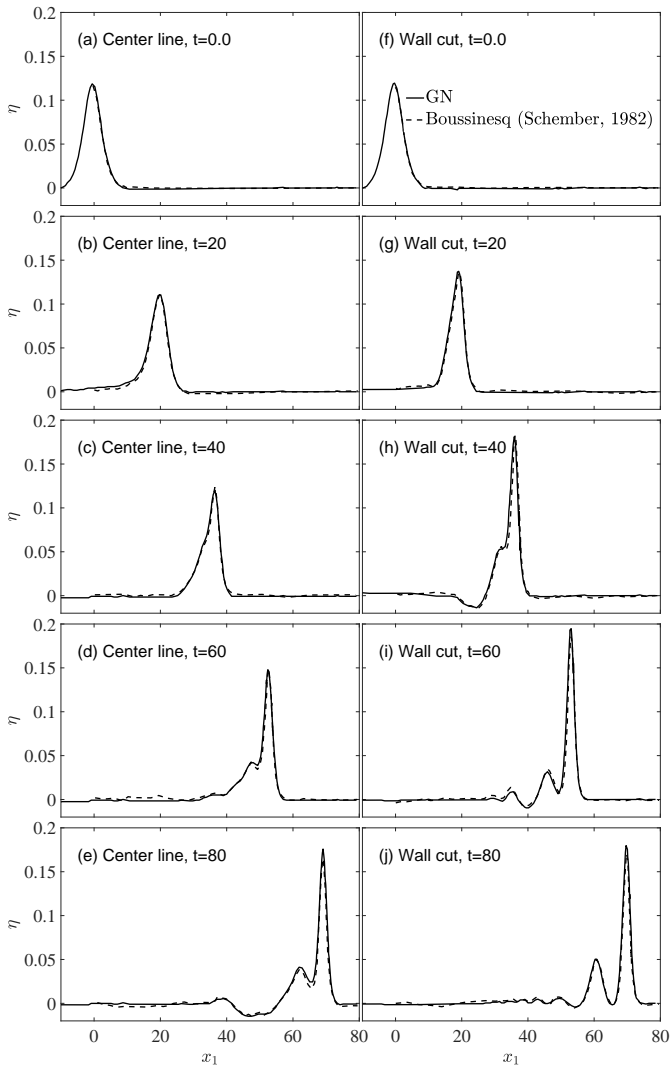


FIGURE 4. Snapshots of surface elevation of solitary wave propagating over the narrow concave ramp (NCR) at the center line (a-e) and wall cut (f-j), calculated by the GN model and compared with the Boussinesq-class results of [25].

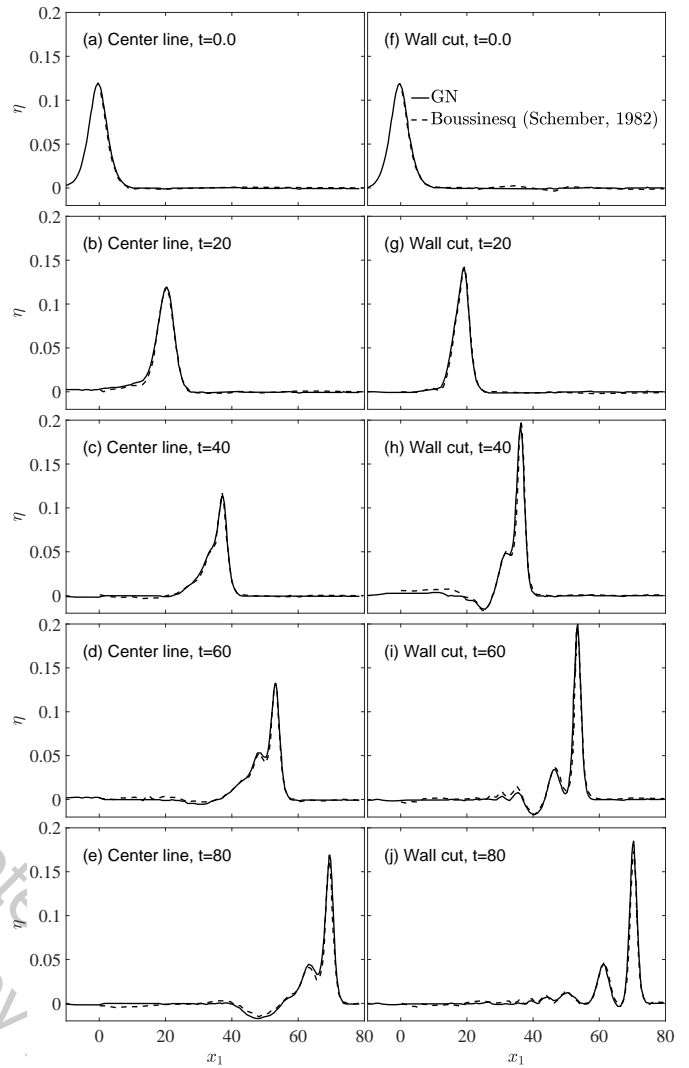


FIGURE 5. Snapshots of surface elevation of solitary wave propagating over the wide concave ramp (WCR) at the center line (a-e) and wall cut (f-j), calculated by the GN model and compared with the Boussinesq-class results of [25].

367 the GN equations are slightly smaller than those reported
 368 by [33], mainly because wave reflection (as large as about
 369 15% in this case, see [27]) is neglected in the KdV models.

370 Cnoidal Wave

371 In this section, results of the GN model for cnoidal
 372 wave propagation over the five bottom ramps are presented.
 373 The wave height and wavelength are $H = 0.12$ and $\lambda = 20$,
 374 respectively. All other variables and numerical setup are
 375 identical to those discussed in the previous sections. Snap-
 376 shots of the 3D surface elevation of cnoidal waves prop-
 377 agating over these ramps obtained by the GN model are
 378 shown in Fig. 9. The cnoidal waves deform significantly as
 379 they propagate over the ramp into the shelf, and this varies

380 in different cases. Qualitatively, similar behaviour in wave
 381 diffraction and refraction is observed as those of a solitary
 382 wave, with the difference that the incoming waves undergo
 383 further deformation due to the interaction with the reflected
 384 waves, and with waves of smaller amplitudes.

385 Concluding Remarks

386 A 3D model for nonlinear wave propagation in shallow
 387 water and over uneven bathymetry is developed based on
 388 the Level I GN equations. A 3D numerical wave tank is
 389 created and a flat, linear ramp is considered in this study.
 390 To further investigate the 3D effects on the wave refraction,
 391 four extensions are added systematically to the flat shelf,
 392 creating concave and convex ramps of different widths. The

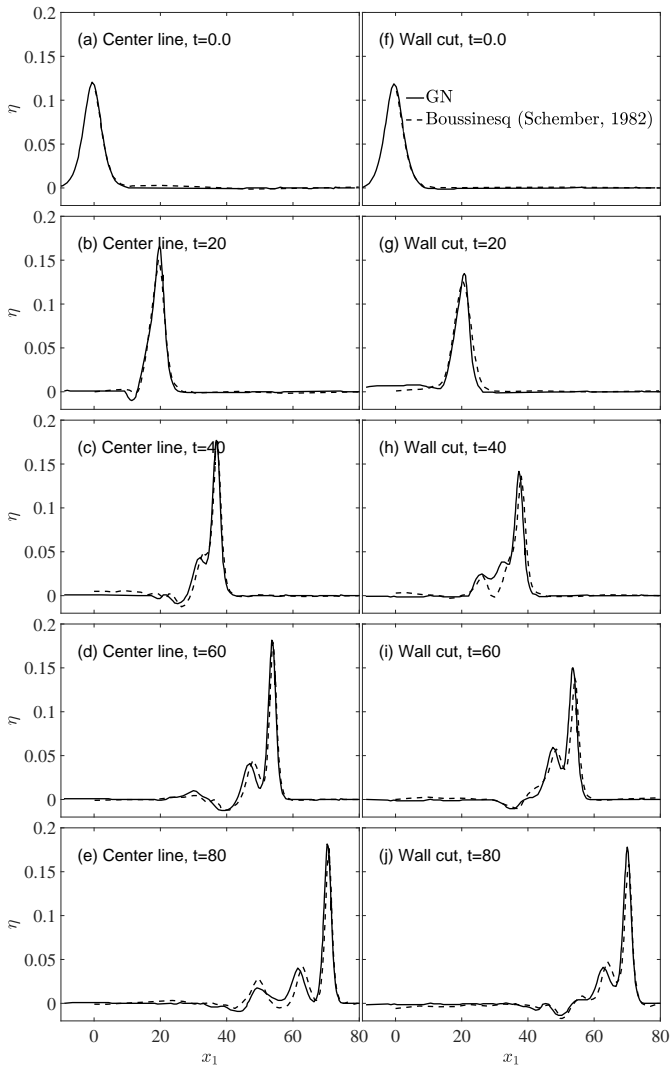


FIGURE 6. Snapshots of surface elevation of solitary wave propagating over the narrow convex ramp (NXR) at the center line (a-e) and wall cut (f-j), calculated by the GN model and compared with the Boussinesq-class results of [25].

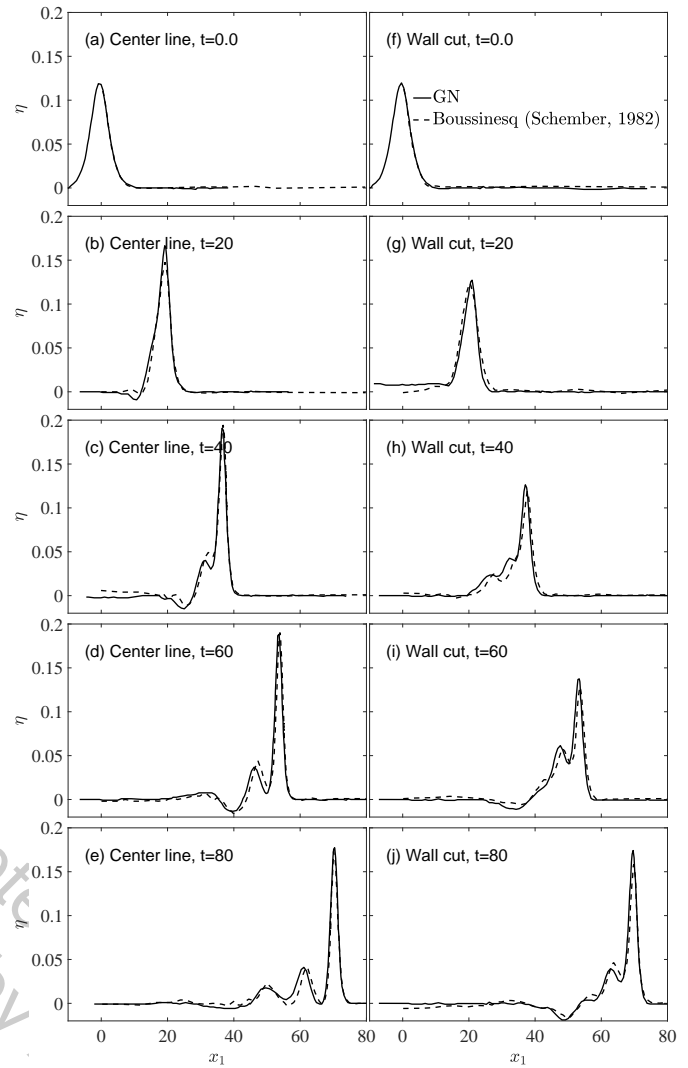


FIGURE 7. Snapshots of surface elevation of solitary wave propagating over the wide convex ramp (WXR) at the center line (a-e) and wall cut (f-j), calculated by the GN model and compared with the Boussinesq-class results of [25].

393 model is used to study solitary and cnoidal wave diffraction
394 and refraction due to various forms of bathymetry.

395 Through the results obtained from the GN model, it is
396 observed that the waves undergo significant deformation as
397 they propagate over the ramps. Common across all cases,
398 the wave amplitude initially increases due to the stronger
399 nonlinearity. The growth of the wave amplitude across the
400 channel width varies depending on the shape of the ramp,
401 such that for concave cases, the wave amplitude is larger at
402 the channel walls, while the wave in the center line is larger
403 for the convex cases. Downwave of the ramp, soliton fission
404 is observed, where second (and sometimes third) solitons
405 are formed. Again the shape of the bathymetry has a
406 significant effect on the magnitude of the second (and third)

407 solitons.

408 It is concluded that the GN equations, capturing non-
409 linearity, dispersion and wave reflection, which also satisfy
410 the boundary conditions exactly, are a remarkable alterna-
411 tive to perturbation-based methods, and a very efficient
412 alternative to any computational fluid dynamics model to
413 study wave transformation in coastal areas.

414 REFERENCES

- 415 [1] Boussinesq, J., 1871. “Théorie de l’intumescence liquide
416 appelée onde solitaire ou de translation”. *Comptes Rendus
417 Acad. Sci. Paris*, **72**, pp. 755–759.
- 418 [2] Rayleigh, L., 1876. “On waves”. *Philosophical Magazine*,
419 **1**(4), pp. 257–279.

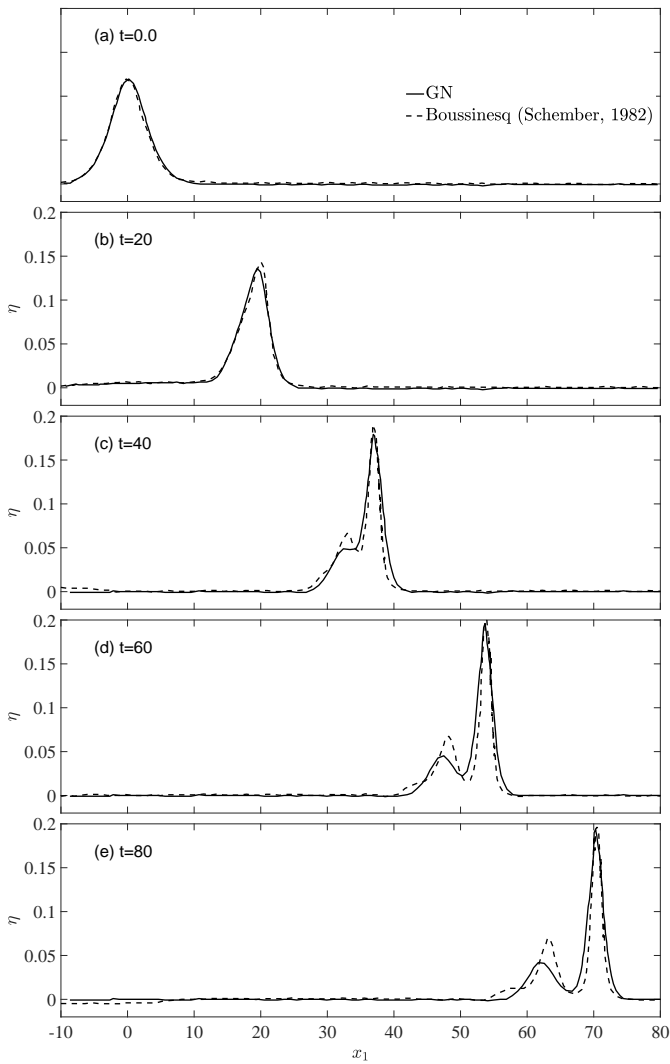


FIGURE 8. Snapshots of surface elevation of solitary wave propagating over the flat linear ramp (FLR), calculated by the GN model and compared with the Boussinesq-class results of [25].

- 420 [3] Korteweg, D., and de Vries, G., 1895. “On the change of
 421 form of long waves advancing in a rectangular canal, and
 422 on a new type of long stationary waves”. *Philosophical
 423 Magazine*, **39**(5), pp. 422–443.
- 424 [4] Laitone, E., 1960. “The second approximation to cnoidal
 425 and solitary waves”. *J. Fluid Mechanics*, **9**(3), pp. 430–
 426 444.
- 427 [5] Madsen, O. S., and Mei, C. C., 1969. “The transforma-
 428 tion of a solitary wave over an uneven bottom”. *J. Fluid
 429 Mechanics*, **39**(4), pp. 781–791.
- 430 [6] Grimshaw, R., 1971. “The solitary wave in water of vari-
 431 able depth. part 2”. *J. Fluid Mechanics*, **46**(3), pp. 611–
 432 622.
- 433 [7] Fenton, J., 1972. “A ninth-order solution for the solitary
 434 wave”. *J. Fluid Mechanics*, **53**(2), pp. 257–271.

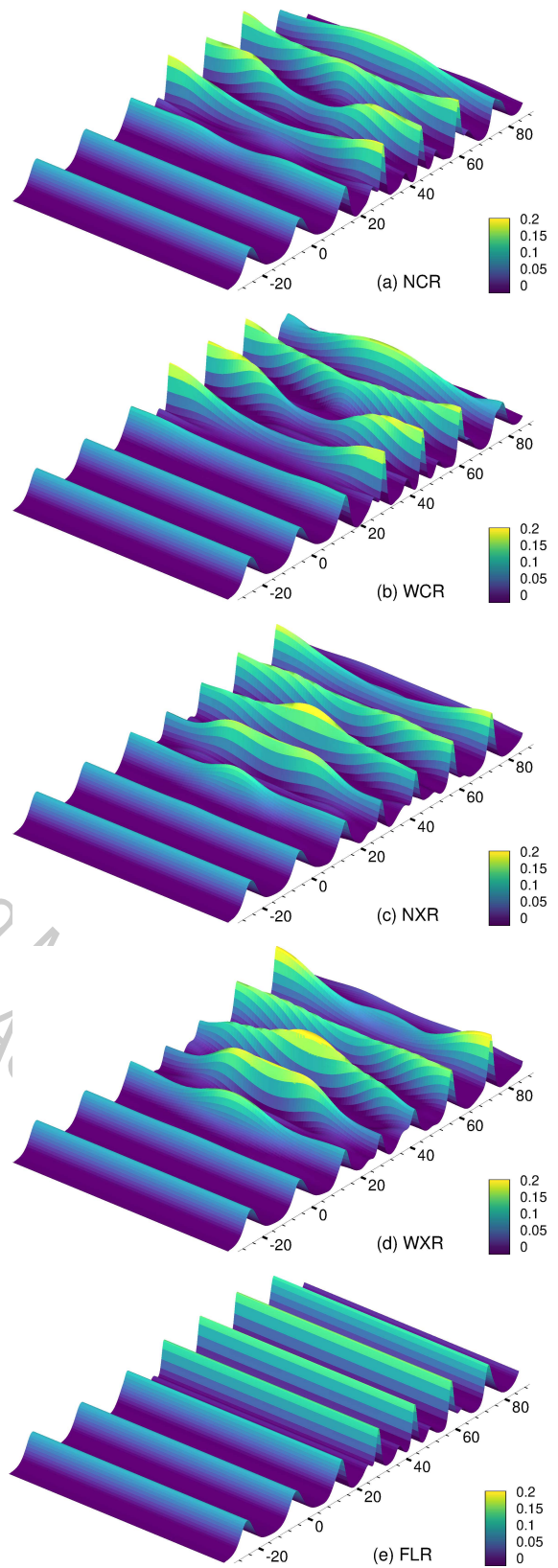


FIGURE 9. Snapshots of the surface elevation of cnoidal waves propagating over (a) NCR, (b) WCR, (c) NXR, (d) WXR, and (e) FLR, taken at time $t=200$. The ramp starts from $x_1 = 6$.

- [8] Wu, T., 1981. “Long waves in ocean and coastal waters”. *Journal of the Engineering Mechanics Division*, **107**(3), May/June, pp. 501–522.
- [9] Liu, P. L.-F., and Losada, I. J., 2002. “Wave propagation modeling in coastal engineering”. *Journal of Hydraulic Research*, **40**(3), pp. 229–240.
- [10] Engsig-Karup, A. P., Bingham, H. B., and Lindberg, O., 2009. “An efficient flexible-order model for 3d nonlinear water waves”. *Journal of computational physics*, **228**(6), pp. 2100–2118.
- [11] Yamazaki, Y., Kowalik, Z., and Cheung, K. F., 2009. “Depth-integrated, non-hydrostatic model for wave breaking and run-up”. *International journal for numerical methods in fluids*, **61**(5), pp. 473–497.
- [12] Roeber, V., Cheung, K. F., and Kobayashi, M. H., 2010. “Shock-capturing boussinesq-type model for nearshore wave processes”. *Coastal Engineering*, **57**(4), pp. 407–423.
- [13] Ma, G., Shi, F., and Kirby, J. T., 2012. “Shock-capturing non-hydrostatic model for fully dispersive surface wave processes”. *Ocean Modelling*, **43**, pp. 22–35.
- [14] Green, A. E., and Naghdi, P. M., 1974. “On the theory of water waves”. *Proc. of the Royal Society of London. Series A, Mathematical and Physical Sciences*, **338**(1612), pp. 43–55.
- [15] Zhao, B. B., Ertekin, R. C., Duan, W. Y., and Hayatdavoodi, M. H., 2014. “On the steady solitary-wave solution of the Green-Naghdi equations of different levels”. *Wave Motion*, **51**(8), pp. 1382–1395.
- [16] Zhao, B. B., Duan, W. Y., Ertekin, R. C., and Hayatdavoodi, M., 2015. “High-level Green–Naghdi wave models for nonlinear wave transformation in three dimensions”. *Journal of Ocean Engineering and Marine Energy*, **1**(2), pp. 121–132.
- [17] Zhao, B. B., Zhang, T. Y., Wang, Z., Duan, W. Y., Ertekin, R. C., and Hayatdavoodi, M., 2019. “Application of three-dimensional IGN-2 equations to wave diffraction problems”. *J. Ocean. Eng. Mar. Energy*, **5**(4), p. 351363.
- [18] Zhao, B. B., Wang, Z., Duan, W., Ertekin, R. C., Hayatdavoodi, M., and Zhang, T., 2020. “Experimental and numerical studies on internal solitary waves with a free surface”. *Journal of Fluid Mechanics*, **899**, p. A17.
- [19] Green, A. E., and Naghdi, P. M., 1976. “A derivation of equations for wave propagation in water of variable depth”. *J. Fluid Mechanics*, **78**, 10, pp. 237–246.
- [20] Ertekin, R. C., 1984. “Soliton generation by moving disturbances in shallow water: Theory, computation and experiment”. PhD thesis, University of California at Berkeley, May, v+352 pp.
- [21] Ertekin, R. C., and Becker, J. M., 1998. “Nonlinear diffraction of waves by a submerged shelf in shallow water”. *J. Offshore Mech. Arct. Eng., ASME*, **120**, November, pp. 212–220.
- [22] Ertekin, R. C., and Sundararaghavan, H., 2003. “Refraction and diffraction of nonlinear waves in coastal waters by the level I Green-Naghdi equations”. In Proc. 22nd Int. Conf. on Offshore Mechanics and Arctic Engineering, OMAE '03, ASME, Cancun, p. 10.
- [23] Hayatdavoodi, M., Neill, D. R., and Ertekin, R. C., 2018. “Diffraction of cnoidal waves by vertical cylinders in shallow water”. *Theoretical and Computational Fluid Dynamics*, **32**(5), pp. 561–591.
- [24] Neill, D. R., Hayatdavoodi, M., and Ertekin, R. C., 2018. “On solitary wave diffraction by multiple, in-line vertical cylinders”. *Nonlinear Dynamics*, **91**(2), pp. 975–994.
- [25] Schember, H. R., 1982. “A new model for three-dimensional nonlinear dispersive long waves”. PhD thesis, California Institute of Technology, Pasadena, CA.
- [26] Ertekin, R. C., and Wehausen, J. V., 1986. “Some soliton calculations”. In *Proc. 16th Symp. on Naval Hydrodynamics, Berkeley*, July, pp. 167-184, Disc. p. 185 (Ed. by W.C. Webster, National Academy Press, Washington, D.C., 1987).
- [27] Ertekin, R. C., Hayatdavoodi, M., and Kim, J. W., 2014. “On some solitary and cnoidal wave diffraction solutions of the Green-Naghdi equations”. *Applied Ocean Research*, **47**, pp. 125–137.
- [28] Hayatdavoodi, M., and Ertekin, R. C., 2015. “Wave forces on a submerged horizontal plate. Part II: Solitary and cnoidal waves”. *J. Fluids and Structures*, **54**(April), pp. 580–596.
- [29] Hayatdavoodi, M., and Ertekin, R. C., 2015. “Nonlinear wave loads on a submerged deck by the Green-Naghdi equations”. *J. Offshore Mechanics and Arctic Engineering*, **137**(1), pp. 011102 (1–9).
- [30] Kostikov, V., Hayatdavoodi, M., and Ertekin, R. C., 2021. “Hydroelastic interaction of nonlinear waves with floating sheets”. *Theor. Comput. Fluid Dyn.*, **35**, pp. 515–537.
- [31] Ursell, F., 1953. “The long-wave paradox in the theory of gravity waves”. *Mathematical Proceedings of the Cambridge Philosophical Society*, **49**(4), pp. 685–694.
- [32] Dhanak, M. R., and Xiros, N. I., 2016. *Springer handbook of ocean engineering*. Springer.
- [33] Johnson, R. S., 1972. “Some numerical solutions of a variable-coefficient Korteweg-de Vries equation (with applications to solitary wave development on a shelf)”. *J. Fluid Mechanics*, **54**, 6, pp. 81–91.